RSC Applied Interfaces

ROYAL SOCIETY OF CHEMISTRY

PAPER

View Article Online
View Journal

Cite this: DOI: 10.1039/d6lf00085a

Photocatalytic reduction of CO_2 with water using catalysts of γ-Ga_2O_3 supported by α-Ga_2O_3: mechanism and roles of each phase

Kosuke Kawaai,[a] Naoto Ota,[b] Shigeo Arai,[c] Muneaki Yamamoto,[c] Tetsuo Tanabe[a] and Tomoko Yoshida *[a]

Gallium oxide (Ga_2O_3), consisting of the mixed phases of α and β, β and γ, and α and γ, is known as a photocatalyst for the reduction of CO_2 with water, producing CO, H_2 and O_2. In previous studies, we investigated Ga_2O_3 consisting of the mixed phases of α-Ga_2O_3 and γ-Ga_2O_3, systematically varying the contents of γ-Ga_2O_3 as catalysts for the photoreduction of CO_2 with water, and proposed a crude reaction mechanism of the photocatalytic reduction of CO_2. However, the mechanism should be refined to clarify the roles of each phase and the effects of the morphology of the mixture. To do this, we have investigated the photocatalytic activity of γ-Ga_2O_3 supported by α-Ga_2O_3 instead of their mixed phases previously examined. With increasing contents of γ-Ga_2O_3, H_2 production rates monotonically decreased, whereas CO production rates increased, reached a maximum at 60–80% of the γ-Ga_2O_3 content, and decreased significantly. These trends are consistent with those observed in the previous studies using the mixed phases. Based on the previously suggested mechanism, we have proposed the detailed mechanism as follows: (1) the surfaces of α-Ga_2O_3 and γ-Ga_2O_3 particles are hydro-oxidated to GaOOH in water, and GaOOH on the γ-Ga_2O_3 particles absorbs CO_2 as bicarbonate; (2) GaOOH on α-Ga_2O_3 is photo-decomposed to α-Ga_2O_3 producing H; (3) the produced H migrates to the γ-Ga_2O_3 particles and reduces the adsorbed bicarbonate to CO; and (4) without UV photons, the surfaces of α-Ga_2O_3 and γ-Ga_2O_3 return to their initial states of GaOOH and bicarbonate-absorbing state, respectively.

Received 13th March 2026,
Accepted 10th April 2026

DOI: 10.1039/d6lf00085a

rsc.li/RSCApplInter

Introduction

Ga_2O_3 is well known as a photocatalyst for CO_2 reduction with water. Among its several different crystalline phases, the α, β, or γ phases have been used in most previous studies. In order to increase the production rate and selectivity of CO among CO_2 reduction products, metallic cocatalysts such as Ag (ref. 1–5) and others[6–8] have often been employed. In our previous work, it has been shown that mixed phases of α and β,[9] α and γ,[10] and β and γ[11] exhibit high photocatalytic activity without the co-catalysts.

In previous work[10] reporting a detailed investigation of the mixed phases of α-Ga_2O_3 and γ-Ga_2O_3 as the photocatalyst of the CO_2 reduction with water, we have suggested the CO_2 reduction mechanism such that water splitting dominates on α-Ga_2O_3 and its H product reduces CO_2 adsorbed on γ-Ga_2O_3 to CO. However, in the mixed phases of α-Ga_2O_3 and γ-Ga_2O_3, it was difficult to control the morphology of the mixture and the particle sizes of both phases.

In order to verify the mechanism, we have investigated the catalytic activity of γ-Ga_2O_3 supported by α-Ga_2O_3 for the photocatalytic CO_2 reduction with water instead of the mixed phases of α-Ga_2O_3 and γ-Ga_2O_3 previously examined. The supported catalysts made it easier to control the contents and morphology of γ-Ga_2O_3 with clear separation of γ-Ga_2O_3 and α-Ga_2O_3. Comparing the present results with the previous results obtained using the mixed phases of α-Ga_2O_3 and γ-Ga_2O_3, we confirm the previously suggested CO_2 reduction mechanism and also provide an improved version. Furthermore, the roles of each phase in the mixed phase samples of the previous work and the present supported samples have been clarified.

Experimental

Experimental procedures

γ-Ga_2O_3 supported by α-Ga_2O_3 photocatalysts (referred to as γ-Ga_2O_3/α-Ga_2O_3 hereafter) were synthesized by an

[a] Department of Energy Engineering, Graduate School of Engineering, Nagoya University, Furo-cho, Chikusa-ku, Nagoya 464-8603, Japan.
E-mail: tyoshida@ energy.nagoya-u.ac.jp; Tel: +81 52 789 5935
[b] Department of Applied Chemistry and Bioengineering, Graduate School of Engineering, Osaka Metropolitan University, Sugimoto 3-3 138, Sumiyoshiku-ku, Osaka 558-8585, Japan
[c] Institute of Materials and Systems for Sustainability, Nagoya University, Furo-cho, Chikusa-ku, Nagoya 464-8603, Japan

impregnation method. Their γ-Ga_2O_3 contents were determined by XAFS analysis, and their morphology (geometrical structure) was observed by transmission electron microscopy (TEM). Specific surface area was measured by the BET method. CO_2 adsorption on γ-Ga_2O_3/α-Ga_2O_3 was also examined by temperature-programmed desorption (TPD). The photocatalytic CO_2 reduction with water under UV light illumination was carried out and analyzed in terms of the γ-Ga_2O_3 content, the morphology, and the specific surface area.

Catalysts preparation

At first, $Ga(NO_3)_3{\cdot}8H_2O$ (KISHIDA Chemical Corporation, purity 99%) was dissolved in distilled water. Then, α-Ga_2O_3 powders, prepared by the calcination of GaOOH at 450 °C for 4 h as reported by Li *et al.*,[12] were dispersed in the solution. The dispersed solution was dried up and calcined at 450 °C for 4 h in air, resulting in γ-Ga_2O_3/α-Ga_2O_3 samples. The contents of γ-Ga_2O_3 (the γ-Ga_2O_3 contents) in γ-Ga_2O_3/α-Ga_2O_3 (nominal contents) were controlled by varying the amounts of $Ga(NO_3)_3{\cdot}8H_2O$ and α-Ga_2O_3.

Photocatalytic CO_2 reduction with water under UV light irradiation

A sample (0.1 g) was dispersed in 100 mL of water with 0.5 M $NaHCO_3$ and stirred in a reaction cell made of quartz. CO_2 gas flowed into the reaction cell at 3 mL min^{-1}. UV light was provided by a Xe lamp through a UV cold mirror. The intensity of the light was 35 mW cm^{-2} at 254 ± 10 nm. The produced gases (mostly H_2, CO, and O_2) were quantified by a gas chromatograph (TCD-GC, Shimadzu GC 8A). The reactions were monitored over five hours to confirm the steady-state production rates of H_2 and CO, which were determined every one hour.

Characterization

The morphology of the samples was observed by TEM, and their specific surface areas were determined by the BET method. Their crystalline structures were determined by X-ray diffraction (XRD) analysis. X-ray absorption analyses (XANES/EXAFS) were also employed and used to determine the γ-Ga_2O_3 contents of the samples.

TEM images were observed with JEM-1000K RS (JEOL Ltd.) under an acceleration voltage of 1000 kV at the High Voltage Electron Microscope Laboratory in Nagoya University. XRD patterns were recorded on Rigaku MiniFlex 600 (Cu Kα radiation, 40 kV, 15 mA) at room temperature. Ga K-edge XANES/EXAFS spectra were measured by the transmission method at room temperature at the 5S1 and 11S2 beam lines at Aichi Synchrotron Radiation Center. The ionization chambers were filled with 100% N_2 for incident X-rays (I_0) and 50% N_2 and 50% Ar for transmitted X-rays (I). Powder samples were set on a masking tape to be thick enough to measure XANES/EXAFS. Specific surface areas were determined by the BET method with N_2 adsorption at −196 °C using a Monosorb™ (Quantachrome). Samples were outgassed at 300 °C for 30 min under N_2 gas flow before measurement. FT-IR spectra were recorded with FT/IR-6100 (JASCO Co.) in the transmission mode at room temperature. Before the measurement, the sample was heated at 400 °C for 1 h. Temperature programmed desorption of CO_2 (CO_2-TPD) was carried out as follows. After drying the sample (50 mg) under He gas flow (50 mL min^{-1}) at 400 °C for 1 h, CO_2 was adsorbed under pure CO_2 gas flow at 40 °C for 1 h. Changing the CO_2 gas flow to a He gas flow (30 mL min^{-1}), CO_2 desorption profiles of the samples were measured, while increasing the temperature from 40 °C to 600 °C at a heating rate of 10 °C min^{-1}.

Results

TEM

Fig. 1 shows the TEM images and the electron diffraction patterns of α-Ga_2O_3 (a), γ-Ga_2O_3 (b), and γ-Ga_2O_3/α-Ga_2O_3 samples (c) and (d). The nominal γ-Ga_2O_3 contents of the last two were 30% and 60%, respectively. As seen in Fig. 1(a), α-Ga_2O_3 consisted of columnar-shaped particles with the length and width of about 1 μm and 0.5 μm, respectively, and each particle was fully crystallized as seen in clear diffraction spots. In contrast, as shown in Fig. 1(b), γ-Ga_2O_3 was composed of aggregates of nm-sized fine particles that were not well crystallized, giving halo rings without any clear spots of the γ-Ga_2O_3. γ-Ga_2O_3/α-Ga_2O_3 samples (Fig. (c) and (d)) clearly show that fine γ-Ga_2O_3 particles exhibiting a halo ring were deposited on the larger columnar-shaped α-Ga_2O_3 particles showing clear diffraction spots. With increasing γ-Ga_2O_3 content, the coverage of γ-Ga_2O_3 particles over the

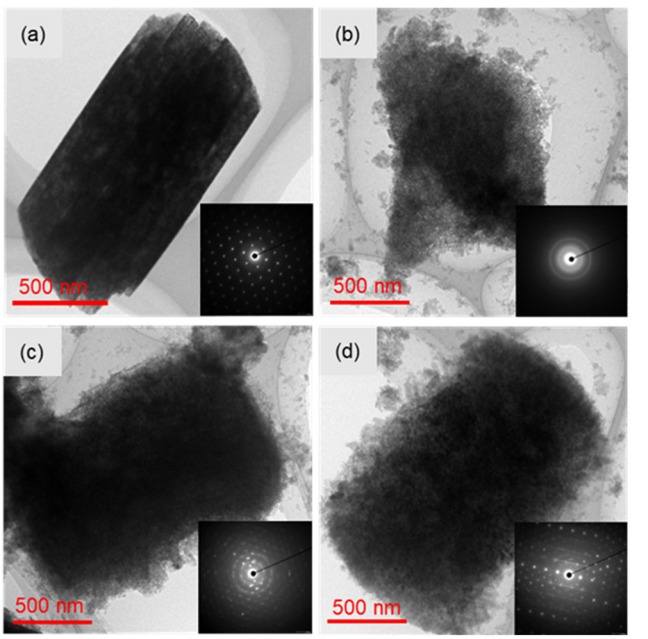

Fig. 1 TEM images and electron diffraction patterns of (a) α-Ga_2O_3, (b) γ-Ga_2O_3, (c) γ-Ga_2O_3/α-Ga_2O_3 (γ = 30%), and (d) γ-Ga_2O_3/α-Ga_2O_3 (γ = 60%).

α-Ga_2O_3 particles increased, but the sizes of the γ-Ga_2O_3 particles hardly changed. In Fig. 1(d), the α-Ga_2O_3 particle was mostly covered by the γ-Ga_2O_3 particles.

XRD

Fig. 2(a) and (b) show the XRD patterns of γ-Ga_2O_3/α-Ga_2O_3, α-Ga_2O_3, and γ-Ga_2O_3 before and after use for the CO_2 reduction, respectively. Most of the sharp peaks were attributed to α-Ga_2O_3, whereas those attributed to γ-Ga_2O_3 were broad, indicating that the α-Ga_2O_3 is well crystallized, while the γ-Ga_2O_3 is poorly crystallized. This corresponds well to the diffraction patterns appearing in Fig. 1. For γ-Ga_2O_3/α-Ga_2O_3, the sharp peaks of α-Ga_2O_3 and the broad peaks of γ-Ga_2O_3 overlapped. Thus, γ-Ga_2O_3/α-Ga_2O_3—consisting of poorly crystallized fine γ-Ga_2O_3 particles supported by larger, fully crystallized α-Ga_2O_3 particles—was synthesized.

As indicated in Fig. 2(b), new peaks appearing in the XRD patterns of the samples after use were attributed to GaOOH. This suggests that the surfaces of Ga_2O_3 particles after use were covered by GaOOH. Such hydro-oxidation of the surface of Ga_2O_3 used as a photocatalyst for CO_2 reduction was reported in previous studies.[9,10]

XAFS

Fig. 3(a) presents the Ga K-edge XANES spectra of α-Ga_2O_3, γ-Ga_2O_3, and γ-Ga_2O_3/α-Ga_2O_3. The differences in XANES fine structures among them were appreciable in the energy range of 10 380–10 480 eV, as shown in the enlarged inset. This allowed us to determine the γ-Ga_2O_3 content of the samples with the linear combination fitting of the XANES spectra as described below. Fig. 3(b) shows an example of the fitting. The fitted spectrum reproduces the experimental spectrum well, giving the compositions of α-Ga_2O_3 and γ-Ga_2O_3 phases of 58% and 42%, respectively.

Fig. 4(a) presents Ga K-edge EXAFS spectra of α-Ga_2O_3, γ-Ga_2O_3, and γ-Ga_2O_3/α-Ga_2O_3, showing clear differences in amplitude and periodicity among the three. This made us apply linear combination fitting used in XANES analysis to

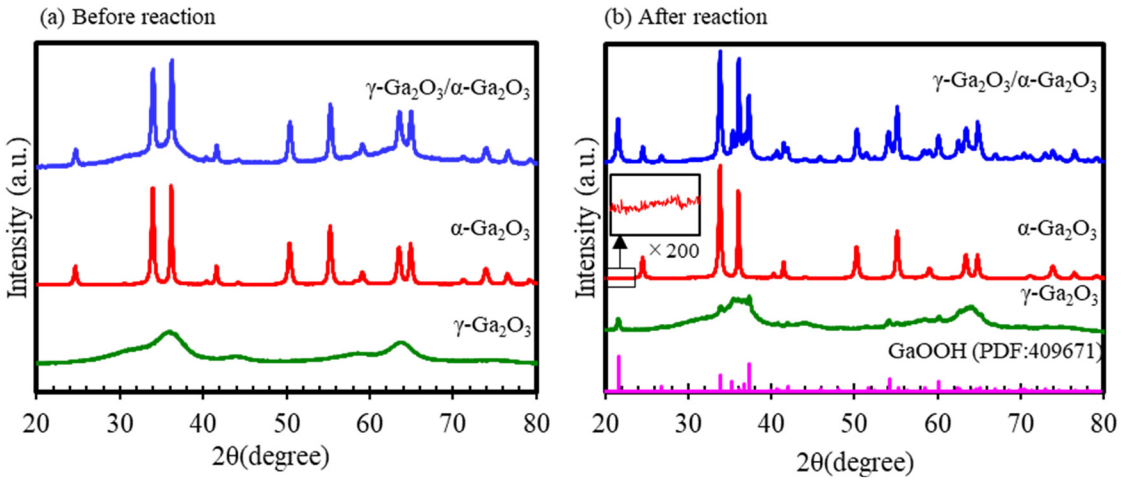

Fig. 2 XRD patterns of γ-Ga_2O_3/α-Ga_2O_3, α-Ga_2O_3, and γ-Ga_2O_3 before (a) and after (b) the reaction. The inset is an enlarged view of the lower-angle side of the α-Ga_2O_3 spectrum to show the appearance of GaOOH.

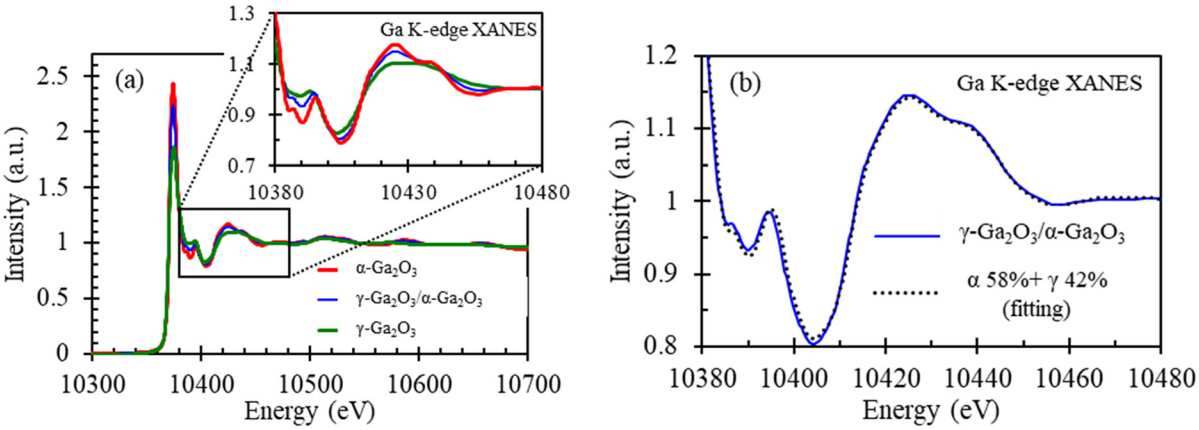

Fig. 3 (a) Ga K-edge XANES spectra of α-Ga_2O_3, γ-Ga_2O_3, and γ-Ga_2O_3/α-Ga_2O_3 samples. (b) Least squares fitting to the observed XANES spectra with a linear combination of the spectra of α-Ga_2O_3 (58%) and γ-Ga_2O_3 (42%).

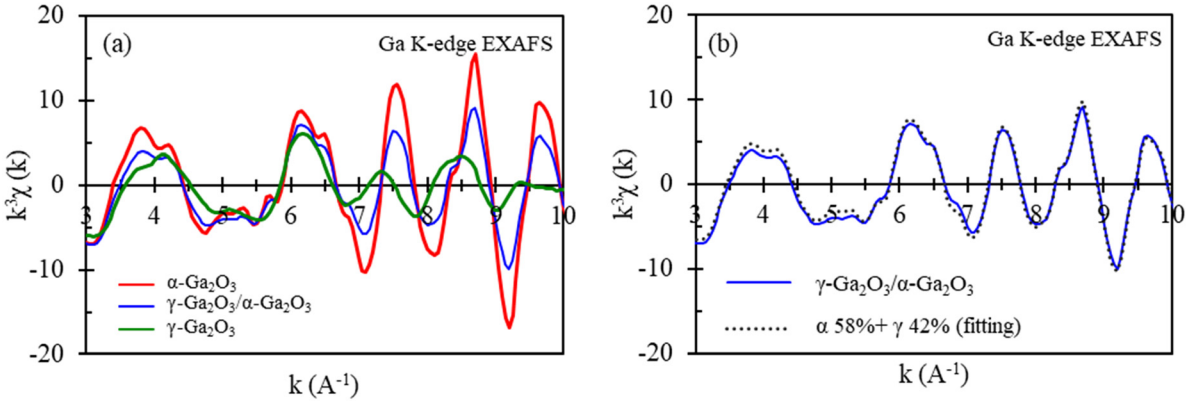

Fig. 4 (a) Ga K-edge EXAFS spectra of α-Ga_2O_3, γ-Ga_2O_3, γ-Ga_2O_3/α-Ga_2O_3 samples. (b) Least squares fitting to the observed EXAFS spectra with a linear combination of the spectra of α-Ga_2O_3 (58%) and γ-Ga_2O_3 (42%).

Table 1 Comparison of the γ-Ga_2O_3 contents determined by least squares fitting using XANES and EXAFS spectra and the nominal states determined for all γ-Ga_2O_3/α-Ga_2O_3 samples

Amount of charge γ (%)		10	20	30	40	50	53	56	60	70	80	83	86	90
Measured γ	XANES (%)	6	10	32	38	42	47	55	58	69	73	77	84	91
	EXAFS (%)	6	10	31	35	43	47	52	55	68	75	79	83	93

determine the γ-Ga_2O_3 contents. Fig. 4(b) shows an example of the fitting with the compositions of α-Ga_2O_3 and γ-Ga_2O_3 phases of 58% and 42%, respectively.

In Table 1, thus determined γ-Ga_2O_3 contents by the XANES and EXAFS analyses are compared with the nominal γ-Ga_2O_3 contents calculated by the mixing ratio of reagents for the synthesis. The determined values agreed within a difference of 3% for all samples.

BET specific surface area

Fig. 5 shows the specific surface areas (SSAs) of all samples determined by the BET method as a function of γ-Ga_2O_3 content determined by XANES analysis. γ-Ga_2O_3 exhibited a much larger SSA than that of α-Ga_2O_3. This is quite reasonable considering the poor crystallinity of γ-Ga_2O_3. The SSA of γ-Ga_2O_3/α-Ga_2O_3 increased with an S-shaped curve showing a slower SSA increase at lower γ-Ga_2O_3 content, a roughly linear increase in the middle range, and saturation over 70% of γ-Ga_2O_3 content. This is different from the linear increase in SSA with the γ-Ga_2O_3 contents for the mixed phases of α-Ga_2O_3 and γ-Ga_2O_3 observed in the previous work.[10]

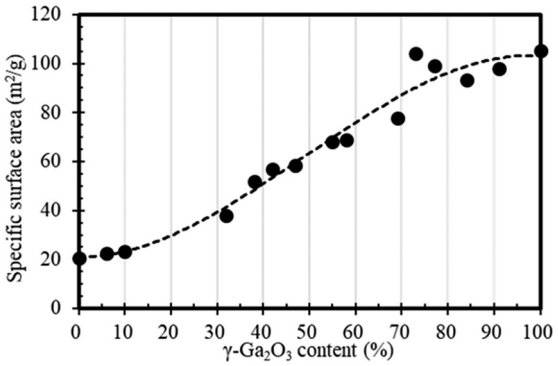

Fig. 5 Changes in BET specific surface area with γ-Ga_2O_3 content (dashed lines serve as a guide to the eyes).

This S-shaped SSA increase corresponds well to the TEM observation. At the low γ-Ga_2O_3 contents, nano-sized γ-Ga_2O_3 particles were deposited discretely without appreciable increase in SSA. In the middle range of γ-Ga_2O_3 content, both SSA and the coverage of the γ-Ga_2O_3 particles, which have a much larger SSA than that of the α-Ga_2O_3 particles, increased linearly until the surface of the α-Ga_2O_3 particles was mostly covered over 70% of the γ-Ga_2O_3 content.

Photocatalytic reduction of CO_2 with water

The reaction products were mostly H_2, CO, and O_2 for all samples. In Fig. 6, the production rates of H_2 and CO against the γ-Ga_2O_3 contents of the samples are plotted. The H_2 production rate was highest for α-Ga_2O_3 and decreased monotonously with increasing γ-Ga_2O_3 content. This is quite consistent with our previous work using the mixed phases of α-Ga_2O_3 and γ-Ga_2O_3 and confirms that the H_2 production is dominated on α-Ga_2O_3. The CO production rates stayed small for lower γ-Ga_2O_3 contents, reached a maximum for samples containing 60–80% of γ-Ga_2O_3, and then decreased markedly for higher γ-Ga_2O_3 contents. This indicates that CO production is promoted by γ-Ga_2O_3, and that the existence of the α-Ga_2O_3 is necessary; that is, γ-Ga_2O_3 alone (without α-Ga_2O_3) showed little activity for the photocatalytic CO_2 reduction with water.

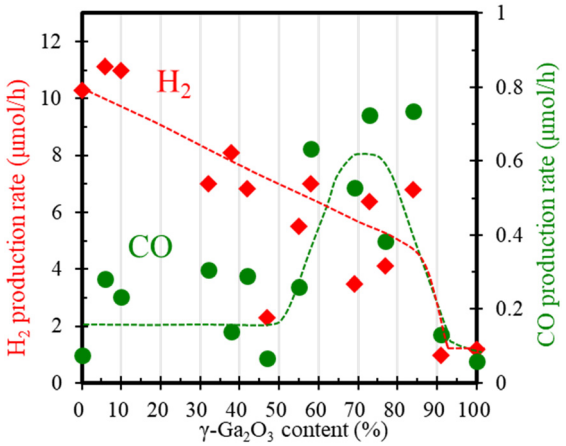

Fig. 6 Production rates of H_2 and CO plotted against the γ-Ga_2O_3 content of γ-Ga_2O_3/α-Ga_2O_3 (dashed lines serve as a guide to the eyes).

CO_2-TPD

Fig. 7 shows the CO_2-TPD profiles of α-Ga_2O_3, γ-Ga_2O_3, and γ-Ga_2O_3/α-Ga_2O_3 (γ = 77%) in the temperature range from 200 °C to 600 °C. Although a desorption peak caused by the adsorbed water appeared under 200 °C, it is not shown in the figure. The adsorbed amounts of CO_2 on γ-Ga_2O_3 and γ-Ga_2O_3/α-Ga_2O_3 were similar and significantly larger than that on α-Ga_2O_3. This indicates that CO_2 adsorption on γ-Ga_2O_3/α-Ga_2O_3 mostly originated from γ-Ga_2O_3.

Considering that CO_2 adsorbed on Ga_2O_3 is known to take mainly two species of carbonate and bicarbonate,[13] the two dominant peaks appeared at around 200–300 °C and 400–500 °C could be attributed to the former and the latter, respectively. This agrees with previous reports showing that, as the precursor of CO forms, the bicarbonate desorbing at higher temperature is more favorable than the carbonate.[13–15] The bicarbonate should be formed through the interaction of CO_2 with OH species on the Ga_2O_3 surface. As depicted in Fig. 2(b), the surface of γ-Ga_2O_3 was converted to GaOOH, which very likely enhanced CO_2 adsorption as the bicarbonate (see (1)).

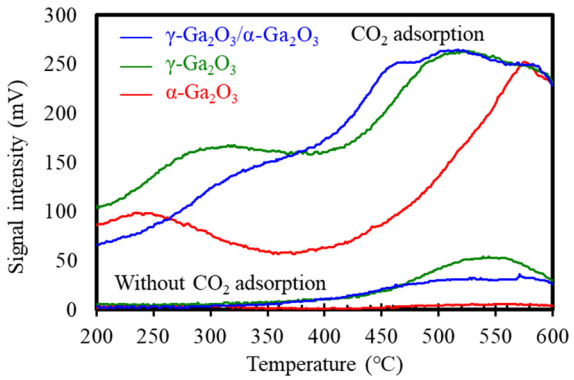

Fig. 7 CO_2-TPD profiles for α-Ga_2O_3, γ-Ga_2O_3 and γ-Ga_2O_3/α-Ga_2O_3 (γ = 77%) samples.

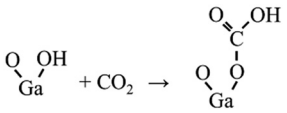

(1)

Discussion

Reaction mechanism

Here, we discuss the mechanism of the photocatalytic CO_2 reduction with water on γ-Ga_2O_3/α-Ga_2O_3. As seen in Fig. 6, H_2 production was dominated on α-Ga_2O_3, while CO production rates increased with the γ-Ga_2O_3 contents and reached a maximum for the samples containing 60–80% of the γ-Ga_2O_3 contents. This observation is quite consistent with the previous work using the mixed phases of α-Ga_2O_3 and γ-Ga_2O_3.[10] Considering the mechanism suggested in the previous work,[10] we have claimed a slightly more detailed mechanism as follows.

I. The surfaces of the α-Ga_2O_3 and γ-Ga_2O_3 particles are hydroxylated to GaOOH in water,

$$Ga_2O_3 + H_2O \rightarrow 2GaOOH \quad (2)$$

and GaOOH on γ-Ga_2O_3 particles absorbs CO_2 a bicarbonate.

II. GaOOH on α-Ga_2O_3 is photo-decomposed to α-Ga_2O_3, producing H, as reported by Aoki *et al.*[9]

$$2GaOOH + h\nu \rightarrow \alpha\text{-}Ga_2O_3 + 2H + O \quad (3)$$

III. The produced H migrates to the γ-Ga_2O_3 particles and reduces the absorbed bicarbonate, resulting in CO. (It is not clear whether this process is photo-assisted or not).

IV. Without photons, the surfaces of α-Ga_2O_3 and γ-Ga_2O_3 return to their initial states of GaOOH and the bicarbonate-absorbing state, respectively.

This mechanism is schematically illustrated in Fig. 8.

Effect of sample morphology on the reaction rate

Although the present results are quite similar to those observed in the previous work using the mixed phases of α-Ga_2O_3 and γ-Ga_2O_3, the present production rates of H_2 and CO were clearly smaller. As seen in Fig. 5, the SSA shows an S-shaped increase with γ-Ga_2O_3 content, while a linear increase was observed in previous work. This seems reasonable considering the morphology difference, whereby

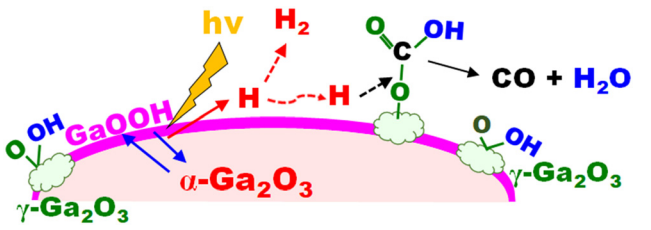

Fig. 8 Schematic drawing of the mechanism of photocatalytic CO_2 reduction with water on γ-Ga_2O_3/α-Ga_2O_3.

the γ-Ga_2O_3 particles cover the α-Ga_2O_3 particles in the present work, while α-Ga_2O_3 and γ-Ga_2O_3 particles were mixed in the previous work. The CO production rates of both studies were hardly correlated with the SSA. This also supports the reaction mechanism described above.

In the present work, the γ-Ga_2O_3 content giving the maximum production rate of CO was around 70%, which was clearly higher than 40% from the previous work, while 0.8 mmol h^{-1} g^{-1} of the former was clearly less than 3 mmol h^{-1} g^{-1} of the latter. This difference could be attributed to the difference in morphology between the supported γ-Ga_2O_3/α-Ga_2O_3 and the mixed phases of α-Ga_2O_3 and γ-Ga_2O_3. Since in the former, the γ-Ga_2O_3 particles cover the α-Ga_2O_3 columnar particles, the surface area of the α particles was comparatively less than that of the latter, resulting in less H production and, consequently, less CO production. In addition, in lower γ-Ga_2O_3 content samples of the former, the γ-Ga_2O_3 particles covered the α-Ga_2O_3 columnar particles rather discretely. Hence, H produced on the α-Ga_2O_3 particles should migrate a longer distance compared with the mixed-phase samples, resulting in less CO production.

There is another geometrical factor. In the mixed phases of α-Ga_2O_3 and γ-Ga_2O_3 samples, both phases are directly exposed to the UV light, whereas in the supported γ-Ga_2O_3/α-Ga_2O_3 photocatalyst, the α-Ga_2O_3 particles are partially or fully covered by the γ-Ga_2O_3 particles. In addition, owing to the smaller band gap of the γ-Ga_2O_3, the γ-Ga_2O_3 particles covering the α-Ga_2O_3 particles would shield the UV light from the α-Ga_2O_3 particle beneath,[16–18] and thus reduce the H formation on the α-Ga_2O_3 particles and consequently lead to lower CO production. These morphological effects further support the proposed reaction mechanism and emphasize the importance of phase arrangement and morphology in determining photocatalytic performance.

Conclusions

In this work, γ-Ga_2O_3 supported by α-Ga_2O_3 (γ-Ga_2O_3/α-Ga_2O_3) photocatalysts with different γ-Ga_2O_3 contents were synthesized by impregnation followed by calcination. TEM and XRD analysis showed that nano-sized γ-Ga_2O_3 particles were deposited on the surface of columnar-shaped α-Ga_2O_3 particles. The γ-Ga_2O_3 content was successfully determined by Ga K-edge XAFS analysis.

Photocatalytic CO_2 reduction with water was carried out to investigate the change in H_2 and CO production rates with γ-Ga_2O_3 content. The H_2 production rate decreased with the γ-Ga_2O_3 content, whereas the CO production rate reached a maximum at 60–80% of γ-Ga_2O_3 content. These results indicate that H_2 production is dominated on α-Ga_2O_3, while CO production is promoted on γ-Ga_2O_3, which absorbs a much larger amount of CO_2 in the form of bicarbonate compared to α-Ga_2O_3.

The changes in the production rates of CO and H_2 with γ-Ga_2O_3 content are consistent with previous work using the mixed phases of α-Ga_2O_3 and γ-Ga_2O_3 as photocatalysts. Based on the previously suggested mechanism, a slightly more detailed mechanism is given as follows: (1) the surface of α-Ga_2O_3 and γ-Ga_2O_3 particles are hydro-oxidated to GaOOH in water, and GaOOH on the γ-Ga_2O_3 particles absorbs CO_2 as bicarbonate; (2) GaOOH on α-Ga_2O_3 is photo-decomposed to α-Ga_2O_3, producing H; (3) the produced H migrates to the γ-Ga_2O_3 particles and reduces the adsorbed bicarbonate to CO. Without UV photons, the surfaces of α-Ga_2O_3 and γ-Ga_2O_3 return to their initial states of GaOOH and bicarbonate-absorbing state, respectively; and (4) without UV photons, the surfaces of α-Ga_2O_3 and γ-Ga_2O_3 return to GaOOH and bicarbonate-absorbing states, respectively. Still, the detailed pathways of CO production are unclear and need to be further researched.

Compared with the mixed phases of α-Ga_2O_3 and γ-Ga_2O_3 photocatalyst reported in the previous study, both H_2 and CO production rates of γ-Ga_2O_3/α-Ga_2O_3 in the present study were lower. This difference is successfully attributed to the difference in the morphology, *i.e.*, g-Ga_2O_3 particles covered the α-Ga_2O_3 particle in the latter, while the mixed phases of α-Ga_2O_3 and γ-Ga_2O_3 particles in the former. These results demonstrate that not only phase composition but also the spatial arrangement of α and γ-Ga_2O_3 plays a crucial role in controlling the CO_2 reduction activity of Ga_2O_3-based photocatalysts.

Conflicts of interest

The authors declare no conflicts of interest.

Data availability

Raw data were generated at Nagoya University. Derived data supporting the findings of this study are available from Tomoko Yoshida on request.

Acknowledgements

This work was supported by JST, CREST Grant Number JP24031877 and JSPS KAKENHI Grant Number JP20KK0116, Japan.

Notes and references

1 M. Yamamoto, T. Yoshida, N. Yamamoto, T. Nomoto, Y. Yamamoto, S. Yagi and H. Yoshida, *J. Mater. Chem. A*, 2015, **3**, 16810.
2 N. Yamamoto, T. Yoshida, S. Yagi, Z. Like, T. Mizutani, S. Ogawa, H. Namiki and H. Yoshida, *e-J. Surf. Sci. Nanotechnol.*, 2014, **12**, 263.
3 Y. Kawaguchi, M. Akatsuka, M. Yamamoto, K. Yoshioka, A. Ozawa, Y. Kato and T. Yoshida, *J. Photochem. Photobiol., A*, 2018, **358**, 459.
4 K. Yoshioka, M. Yamamoto, T. Tanabe and T. Yoshida, *e-J. Surf. Sci. Nanotechnol.*, 2020, **18**, 168.

5 M. Yamamoto, S. Yagi and T. Yoshida, *Catal. Today*, 2018, **303**, 334.
6 Y. Pan, Z. Sun, H. Cong, Y. Men, S. Xin, J. Song and S. Yu, *Nano Res.*, 2016, **9**, 1689.
7 S. Kikkawa, K. Teramura, H. Asakura, S. Hosokawa and T. Tanaka, *J. Phys. Chem. C*, 2018, **122**, 21132.
8 H. Yoon, J. Yang, S. Park, C. Rhee and Y. Sohn, *Appl. Surf. Sci.*, 2021, **536**, 147753.
9 T. Aoki, M. Yamamoto, T. Tanabe and T. Yoshida, *New J. Chem.*, 2022, **46**, 3207.
10 N. Ota, Y. Takashiro, M. Yamamoto, T. Tanabe and T. Yoshida, *J. Mater. Chem. A*, 2025, **13**, 6663.
11 M. Akatsuka, Y. Kawaguchi, R. Itoh, A. Ozawa, M. Yamamoto, T. Tanabe and T. Yoshida, *Appl. Catal., B*, 2020, **262**, 118247.
12 L. Li, W. Wei and M. Behrens, *Solid State Sci.*, 2012, **14**, 971.
13 B. Zhao, Y. Pan and C. Liu, *Catal. Today*, 2012, **194**, 60.
14 K. Teramura, K. Hori, Y. Terao, Z. Huang, S. Iguchi, Z. Wang, H. Asakura, S. Hosokawa and T. Tanaka, *J. Phys. Chem. C*, 2017, **121**, 8711.
15 Y. Wang, Y. Sun, X. Liu and F. Dong, *PNAS Nexus*, 2024, **3**, 339.
16 J. Lyons, *ECS J. Solid State Sci. Technol.*, 2019, **8**, 3226.
17 T. Oshima, T. Nakazono, A. Mukai and A. Ohtomo, *J. Cryst. Growth*, 2012, **359**, 60.
18 D. Shinohara and S. Fujita, *Jpn. J. Appl. Phys.*, 2008, **47**, 7311.